

CHAPTER 48

APPLICABILITY OF A NEW HYBRID PARAMETRIC WAVE PREDICTION MODEL

Yoshio Hatada¹ and Masataka Yamaguchi²

ABSTRACT

DOLPHIN-I is a new hybrid parametric deep water wave prediction model developed by the authors. This paper examines the applicability of DOLPHIN-I, on the basis of the comparison of the computation with the data of significant waves obtained in five sea areas with different horizontal scales around Japan during monsoons and typhoons. In particular, the wave data in Osaka Bay includes frequency and directional spectra. It is verified that the model practicality is excellent, because it reproduces well the wave data observed in any concerned sea area.

1. INTRODUCTION

In the past 10 years, a number of hybrid parametric wave prediction models such as HYP A, TOHOKU, GONO (SWAMP, 1985), HYPAS (Günther et al., 1984) and Graber & Madsen's model (1988) have been proposed. The advantages of these models which imply the effects of wind input, wave-wave interaction and wave breaking in a parametric representation, are the capability to save computer processing time, as compared with the discrete spectral model, and to give reasonable estimation of wave growth under a gradually-varying simple wind field.

However, the degree of freedom in the models is not enough to properly resolve the directional characteristics of a confused wave field in the rapidly-varying wind field of a typhoon and in the sea area enclosed by complicated shorelines, because wave direction is approxi-

1 Research Assistant, Dept. of Ocean Eng., Ehime Univ., Bunkyocho 3, Matsuyama 790, Ehime Pref., Japan

2 Prof., Dept. of Ocean Eng., Ehime Univ., Bunkyocho 3, Matsuyama 790, Ehime Pref., Japan

mated by only one parameter such as a mean wave direction averaged with respect to frequency and direction.

Yamaguchi et al.(1988) developed a new directionally-decoupled hybrid parametric wave prediction model in deep water, hereafter referred to as DOLPHIN-I, in order to improve this situation. DOLPHIN-I assumes that the directional energy of wind-sea defined separately for each direction grows according to a parametric equation derived from an analysis of observed wave growth data under the assumption of ideal generation conditions and that each swell component propagates independently, undergoing energy dissipation. It is formulated so as to make it possible to estimate the time variation of directional spectra at a prescribed location through the computation along the straight wave rays focusing at the location. The computed results for test cases given in SWAMP(1985) showed physically sound behavior in each case (Yamaguchi et al., 1988).

The aim of this paper is to examine the applicability of DOLPHIN-I, based on the comparison between computation and observation. First, a brief explanation of the model is provided from the view points of model formulation and computation method. Wave hindcast is conducted in five sea areas with different horizontal scales during monsoons and typhoons, and wave observation data used in the comparison include not only significant waves but also frequency and directional spectra.

2. OUTLINE OF DOLPHIN-I

(1) Model Formulation

The radiative transfer equation is given as

$$\frac{\partial E(f, \theta)}{\partial t} + C_g(f) \cos \theta \frac{\partial E(f, \theta)}{\partial x} + C_g(f) \sin \theta \frac{\partial E(f, \theta)}{\partial y} = G(f, \theta) \quad (1)$$

where $E(f, \theta)$ is the directional spectrum, f the frequency, θ the direction, $C_g(f) (= g/4\pi f)$ the group velocity of a wave component, g the acceleration of gravity and $G(f, \theta)$ the source function modeling inflow and outflow of wave energy. When a straight propagation path of a wave component is selected such that $dx/ds = \cos \theta$ and $dy/ds = \sin \theta$, Eq.(1) is rewritten as

$$\frac{\partial E(f, \theta)}{\partial t} + \frac{\partial C_g(f) E(f, \theta)}{\partial s} = G(f, \theta) \quad (2)$$

The integration of Eq. (2) over frequency yields the following equation which describes the evolution of directional energy density of wind waves $E(\theta)$

$$\left. \begin{aligned} \frac{\partial E(\theta)}{\partial t} + \frac{\partial \bar{C}_g E(\theta)}{\partial s} &= \int_0^\infty G(f, \theta) df \\ E(\theta) &= \int_0^\infty E(f, \theta) df, \quad \bar{C}_g = \int_0^\infty C_g(f) E(f, \theta) df / E(\theta) \end{aligned} \right\} \quad (3)$$

where \bar{C}_g is the frequency-averaged group velocity.

We assume that wind waves grow under the ideal generation condition, in which case directional spectrum is expressed as a product of the JONSWAP spectrum (Hasselmann et al., 1973) and $\cos^4\theta$ -type angular spreading function and that evolutions of spectral parameters such as saturation range constant α , dimensionless peak frequency ν , and peak enhancement factor γ are governed by the energy-dependent relations which are derived from the empirical expressions of Mitsuyasu et al. (1980). Then, the frequency-averaged group velocity and source function in Eq. (3) can be determined, and evolution of the directional energy of wind-sea $E^*(\theta)$ is described as

$$\left. \begin{aligned} \frac{\partial E^*(\theta)}{\partial t} + \frac{\partial}{\partial s} [C_g(f_m) f(\gamma) E^*(\theta)] &= 2.851 \times 10^{-4} \left\{ \frac{E^*(\theta)}{D^*(\theta)} \right\}^{0.3273} \cdot \exp \left[-0.0875 \right. \\ &\cdot \left. \left\{ \frac{E^*(\theta) |D^*(\theta)|}{1.43 \times 10^3 - E^*(\theta) |D^*(\theta)|} \right\}^{0.8542} \right] \cdot \frac{u_*^3}{g} \cos(\theta - \theta_w) D^*(\theta) \\ D^*(\theta) &= \begin{cases} (8/3 \pi) \cos^4(\theta - \theta_w); & |\theta - \theta_w| < \pi/2 \\ 0 & ; |\theta - \theta_w| \geq \pi/2 \end{cases} \\ f(\gamma) &= 0.8572 \gamma^{0.0426} \end{aligned} \right\} \quad (4)$$

where f_m is the peak frequency, u_* the friction velocity, θ_w the wind direction and $D(\theta)$ the angular spreading function. The asterisk means the ideal generation condition.

Propagation of a swell component is formulated by the above-mentioned one-dimensional radiative transfer equation with an energy dissipation term. It is given as

$$\frac{\partial E_s(f, \theta)}{\partial t} + \frac{\partial C_g(f) E_s(f, \theta)}{\partial s} = \begin{cases} -0.25(u_*|C|)^2 f E_s(f, \theta); & |\theta - \theta_w| < \pi/2 \\ -\beta_M(f, \theta) E_s(f, \theta) & ; |\theta - \theta_w| \geq \pi/2 \end{cases} \quad (5)$$

where $E_s(f, \theta)$ is the directional spectrum of a swell component, $C (=g/2\pi f)$ the wave celerity, and β_M the damping rate due to opposing wind.

In the general sea state, directional spectra of sea waves $E(f, \theta)$ are divided into frequency-integrated directional energy of wind-sea $E_s(\theta)$ and directional spectra of swell components $E_s(f, \theta)$. The directional energy of wind-sea is defined by

$$E_s(\theta) = \int_{f_{m0}}^\infty E(f, \theta) df \quad (6)$$

where $f_{m\theta}$ is the peak frequency of directional spectra for each direction and $\delta(=0.6)$ the correction factor used for the separation of wind-sea and swell. Setting $E_\delta(\theta)$ equal to $E^*(\theta)$ at the growth stage of wind-sea, evolution of wind-sea energy for each direction is computed from Eq. (4) and then total wave energy parameter of wind-sea $\tilde{\epsilon}^*$ is evaluated by $\tilde{\epsilon}^* = E^*(\theta)/D^*(\theta)$. Directional spectra of wind-sea $E_w(f, \theta)$ are established using both the JONSWAP spectrum with the spectral parameters related to dimensionless wave energy and the angular spreading function $D^*(\theta)$. On the other hand, change of directional spectrum for each swell component $E_s(f, \theta)$ is obtained from Eq. (5).

Directional spectrum in general sea state at the same place is evaluated by simply summing up the directional spectral component for the same frequency and direction of both wind sea and swell as

$$E(f, \theta) = E_w(f, \theta) + E_s(f, \theta) \tag{7}$$

The wave statistics are obtained by the numerical integration of directional spectra over wave direction and frequency using the relations such as

$$\left. \begin{aligned} E(f) &= \int_0^\pi E(f, \theta) d\theta, \quad \epsilon = \int_0^\infty E(f) df, \quad H_{1/3} = 4\sqrt{\epsilon} \\ T_{1/3} &= 1.20\sqrt{\epsilon / \int_0^\infty f^2 E(f) df}, \quad \bar{\theta} = \tan^{-1} \left\{ \frac{\int_0^\infty \int_0^\pi E(f, \theta) \sin \theta d\theta df}{\int_0^\infty \int_0^\pi E(f, \theta) \cos \theta d\theta df} \right\} \end{aligned} \right\} \tag{8}$$

where $E(f)$ is the frequency spectrum, ϵ the total wave energy, $H_{1/3}$ the significant wave height, $T_{1/3}$ the significant wave period, and $\bar{\theta}$ the mean wave direction.

(2) Method of Numerical Computation

DOLPHIN-I estimates the time variation of directional spectra of sea waves at a prescribed point by following growth, decay, and propagation of sea waves along a wave ray radiating separately from the point for each direction, as shown in Fig. 1.

The evolution equation of directional energy, Eq. (4) is solved by a finite difference method of the two-step Lax-Wendroff scheme. It is given as

$$\left. \begin{aligned} e_{i+1/2}^{n+1/2} &= \frac{e_i^n + e_{i+1}^n}{2} - \frac{\Delta t}{2 \Delta s} (K_{i+1}^n - K_i^n) + Q_{i+1/2}^n \frac{\Delta t}{2} \\ e_i^{n+1} &= e_i^n - \frac{\Delta t}{\Delta s} (K_{i+1/2}^{n+1/2} - K_{i-1/2}^{n+1/2}) + Q_i^{n+1/2} \Delta t \end{aligned} \right\} \tag{9}$$

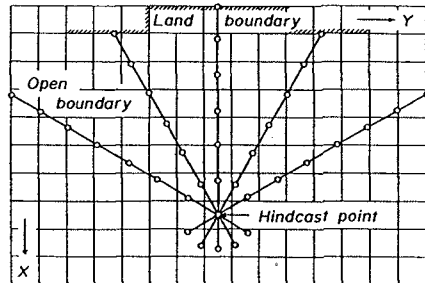


Fig. 1 Wave ray and computation of propagation.

where $e = E^*(\theta)$, $K = \overline{C_g} E^*(\theta)$, Q is the source term in Eq.(4), n the index of the time step, i the grid number on a wave ray, and Δs the grid spacing on a wave ray. The value of e is specified in a parametric manner at the upwave open boundary and it is set at zero in the case of the land boundary. At the downwave boundary, directional energy is freely transmitted, and the upwind difference scheme indicated by

$$e_N^{n+1} = e_N^n - \frac{\Delta t}{\Delta s} (K_N^n - K_{N-1}^n) + Q_N^n \Delta t \tag{10}$$

is used, because Eq. (9) is not applicable, where N is the grid number at the boundary. It should be noted that one grid point is added to the grid system for each direction in order to keep the accuracy of computation at the hindcast point.

The computation of the radiative transfer equation, Eq. (5), makes use of a fractional time step method in which the propagation equation and the forcing equation are solved alternatively. The propagation step uses a piecewise ray method with the Lagrange third order spatial interpolation formula expressed as

$$\left. \begin{aligned} E_s(f, \theta) &= a_1 E_{s_{i-2}}^n(f, \theta) + a_2 E_{s_{i-1}}^n(f, \theta) + a_3 E_{s_i}^n(f, \theta) + a_4 E_{s_{i+1}}^n(f, \theta) \\ a_1 &= -(r-2)(r-1)r/6, \quad a_2 = (r-2)(r-1)(r+1)/2, \\ a_3 &= -(r-2)r(r+1)/2, \quad a_4 = (r-1)r(r+1)/6, \quad r = 1 - C_d(f)\Delta t/\Delta s \end{aligned} \right\} \tag{11}$$

At the grid point next to the upwave boundary and at the downwave boundary, the interpolation formulas with the first and second order accuracy

$$\left. \begin{aligned} E_s(f, \theta) &= (1-r)E_{s_i}^n(f, \theta) + rE_{s_{i+1}}^n(f, \theta) \\ E_s(f, \theta) &= a'_1 E_{s_{i-2}}^n(f, \theta) + a'_2 E_{s_{i-1}}^n(f, \theta) + a'_3 E_{s_i}^n(f, \theta) \\ a'_1 &= (r-1)r/2, \quad a'_2 = (1-r)(1+r), \quad a'_3 = r(r+1)/2 \end{aligned} \right\} \tag{12}$$

are applied respectively as well as in the above-mentioned case. The computation of the forcing step is conducted with the analytical solution given by

$$\left. \begin{aligned} E_s^{n+1}(f, \theta) &= E_s(f, \theta) \exp\{-0.25(u_*^2/C)^2 f \Delta t\} \quad ; \quad |\theta - \theta_w| < \pi/2 \\ E_s^{n+1}(f, \theta) &= E_s(f, \theta) \exp(-\beta_w \Delta t) \quad ; \quad |\theta - \theta_w| \geq \pi/2 \end{aligned} \right\} \tag{13}$$

3. APPLICABILITY OF DOLPHIN-I

(1) Conditions in Wave Hindcast

As shown in Fig. 2, wave hindcast is conducted in the five sea areas with different horizontal scales: Lake Biwa with an extension of 15 to 30 km, Osaka Bay and the Kii Channel with an extension of 30 to 100 km, the western part of the Seto Inland Sea with an extension of 150 km, the Japan Sea with an extension of 800 to 1300 km, and the Northwest Pacific Ocean with an extension of more than 2000 km. In the Pacific Ocean, typhoon-generated waves are hindcast, in which case wind distribution is

estimated by a simple parametric typhoon model. In the other sea areas, waves associated with monsoons are computed, in which case evaluation of wind distribution over the sea is based on a spatial interpolation method of the measured wind data or a weather map analysis.

Table 1 is the computational conditions used in wave hindcast on each sea area. The directional range of -180° to 180° , number of directional data N_θ of 37 and directional increment $\Delta\theta$ of 10° are the same in all cases.

Wind velocity at the height of 10 m over sea level U_{10} in each sea area is estimated with the method given in Table 1. Friction velocity u_* in DOLPHIN-I is computed from U_{10} by use of a modified form of Mitsuyasu's empirical formula (1984). It is written as

$$C_d = (u_* / U_{10})^2 = \begin{cases} (0.581 + 0.063 U_{10}) \times 10^{-3} & ; U_{10} \geq 10 \text{ m/s} \\ 1.211 \times 10^{-3} & ; U_{10} < 10 \text{ m/s} \end{cases} \quad (14)$$

where C_d is the drag coefficient of the sea surface. Wind characteristics at grid points on each wave ray are evaluated every 30 minutes through linear interpolations with respect to time and space of wind data given every 1 hour at the rectangular grid points.

Table 1 Numerical conditions used in wave hindcast.

| | Lake Biwa | Osaka Bay & Kii Chan. | Seto Inland Sea | Japan Sea | Pacific Ocean |
|---------------------------|---------------------------------|-----------------------|-----------------|----------------------|---------------|
| MxN | 20x15 | 36x28 | 30x35 | 25x44 | 43x43 |
| $\Delta x = \Delta y$ km | 2.5 | 3 | 5 | 40 | 80 |
| Δs km | 2.5 | 3 | 5 | 40 | 80 |
| Δt min | 7.5 | 6 | 10 | 30 | 60 |
| f_{\min} Hz | 0.176 | 0.1 | 0.1 | 0.05 | 0.04 |
| f_{\max} Hz | 2 | 1.5 | 1.5 | 1 | 1 |
| N_f | 22 | 23 | 23 | 24 | 30 |
| method of wind estimation | interpolation of measured winds | ditto | ditto | weather map analysis | typhoon model |

M, N: number of grids in x and y direction, Δx , Δy : grid spacing
 Δs : grid spacing on a ray, Δt : time increment, N_f : number of frequency
 f_{\min} : minimum frequency, f_{\max} : maximum frequency

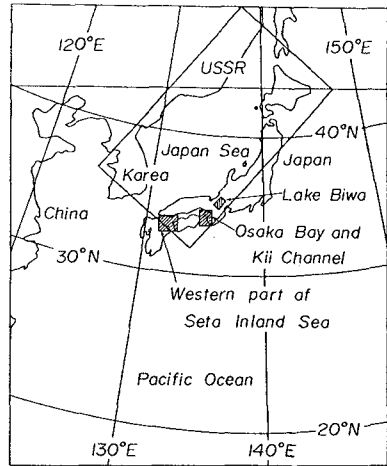


Fig. 2 Five sea areas with different horizontal scales used in wave hindcast.

In the hindcast on the sea areas, except for the Pacific Ocean, land boundary condition in which case the directional spectrum is zero is imposed. On the other hand, directional spectra computed by a product of JON-SWAP-type frequency spectrum referred to as the Ross hurricane model(1976) and $\cos^4\theta$ -type angular spreading function are given at the grid points corresponding to the open boundary of the Pacific Ocean area, in which case input data are local wind characteristics and distance between the concerned grid point and the position of the typhoon center.

In order to initiate DOLPHIN-I, which does not have any term for initial generation of wind waves, directional spectra computed from the before-mentioned model under the conditions of $H_{1/3} = 0.1$ m and $u_* = 0.12$ m/s are provided as an initial condition.

(2) Wave Hindcast in Lake Biwa

Fig. 3 shows the grid system with spacing of 2.5 km placed over Lake Biwa. During winter monsoons, strong winds of more than 10 m/s continue to blow over the lake for two or three days with repetitions of gradual increase and decrease of wind velocity, and the resulting wind fields are quasi-homogeneous and quasi-steady. The wind distribution is obtained by linear interpolation of the wind data measured at three points(B, C and D) with respect to the y direction, in which case uniformity of the wind field in the x direction is assumed.

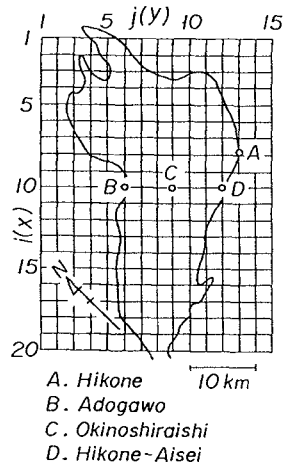


Fig. 3 Grid system used in Lake Biwa.

Fig. 4 indicates the comparison between time variations of significant wave heights and

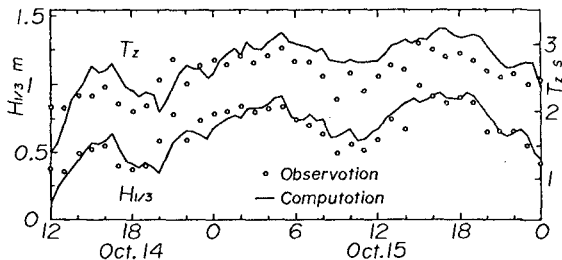


Fig. 4 Comparison between the computed and observed significant waves in Lake Biwa.

mean wave periods observed and hindcast at Hikone-Aisei point, where T_z is the mean period defined by the zero and second moments of frequency spectra, as is indicated in Eq. (10). This is typical of wave variations occurring during seasonal winds in Lake Biwa. The figure shows excellent agreement between the computation and the measurement of significant wave height variation, but hindcast mean periods are slightly greater than the observed results. The reason is that the formulation of DOLPHIN-I is based on Mitsuyasus's empirical relation between spectral parameters and dimensionless fetch, which gives smaller estimation than spectral parameters obtained from the analysis of wave data in Lake Biwa. So, improvement of the model applicability to wave evaluation in Lake Biwa is possible by changing the expressions of spectral parameters.

(3) Wave Hindcast in Osaka Bay and the Kii Channel

Fig. 5 is the grid system with a spacing of 5 km used in wave hindcast, in which small circles are the wind observation stations deployed around the concerned sea area. Wind distribution over the area every 1 hour is estimated from the application of a linear interpolation formula to measured wind data on each of the triangular meshes made by connecting the wind observation stations together (Yamaguchi et al., 1981).

Fig. 6 is the comparison between the computation and the observation for time variation of significant waves at the MT station in Osaka Bay during a strong storm brought about with a typical pressure pattern in the winter of Japan. Wave heights show rapid growth to over 2 m high because of the duration of strong winds of maximum 20 m/s with the direction of SW to W and then they reduce to about 1 m high with a change into moderate winds of 10 m/s or so with the direction of WNW, while wave periods of about 4 s do not vary so much as wave heights. DOLPHIN-I reproduces well the observed time variation of wave heights, but gives a slight overestimation of that

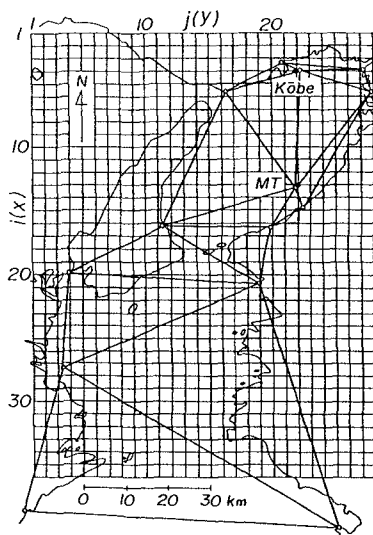


Fig. 5 Grid system used in Osaka Bay and the Kii Channel.

of wave periods.

Another comparison of the time variation of significant waves at the MT station is indicated in Fig. 7. Strong stormy winds during the period of wave hindcast were brought about by a developing low system which proceeded easterly over the Japan Sea. DOLPHIN-I again results in good resolution for the observed time variation of significant waves associated with strong winds whose velocity increases rapidly and then decreases with change of the wind direction from SW to NW. But in detail, DOLPHIN-I tends to give a slight underestimation before the peak period of the storm.

Fig. 8 is the comparison between the computation and the observation for frequency spectra and directional spectra at the MT station. DOLPHIN-I behaves well even for reproduction of the observed wave spectra, but the directional spectra in measurement have a smoother distribution than those in computation, because the directional spectra are evaluated with the Fourier series method of poor directional resolution from current records of the three components. A slight difference in the dominant wave direction in directional spectrum is also found because of possible errors in orientation of the instrument and variability of the measured wind direction.

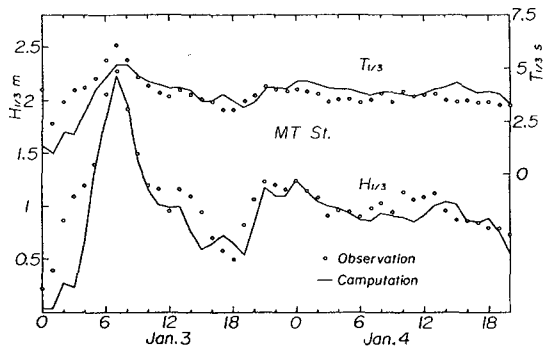


Fig. 6 Comparison between the computed and observed significant waves at the MT station in Osaka Bay (1).

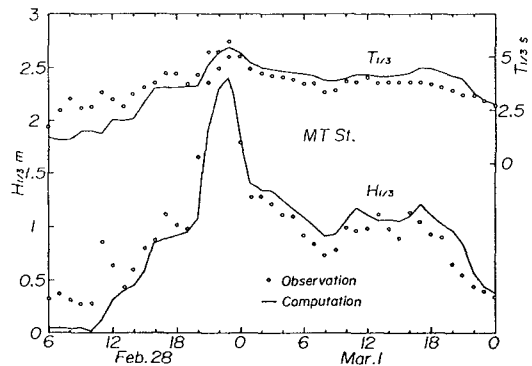


Fig. 7 Comparison between the computed and observed significant waves at the MT station in Osaka Bay (2).

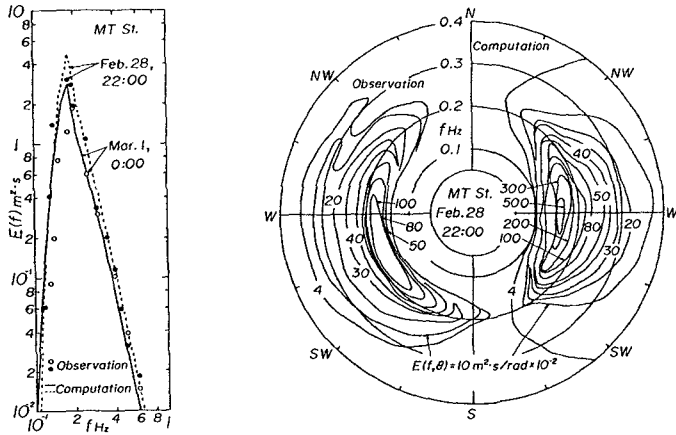


Fig. 8 Comparison of the computed and observed frequency spectra and directional spectra at the MT station in Osaka Bay.

(4) Wave Hindcast in the Western Part of the Seto Inland Sea

Wave hindcast in this sea area is conducted for the period of seasonal winds on the grid system given in Fig. 9, in which case estimation of wind distribution is based on a linear interpolation of measured wind data on triangular elements as well as the case for Osaka Bay. The seasonal winds occurred with the passage of twin low pressure systems over the Japan Sea and the resulting moderately strong winds of over 10 m/s with the direction of WNW to NW continued to blow over the sea area.

Fig. 10 is a simultaneous plot of the time variations of the significant waves at Kanda and Iyo obtained from the computation and the observation. At Kanda with longer fetch for predominant wind direction,

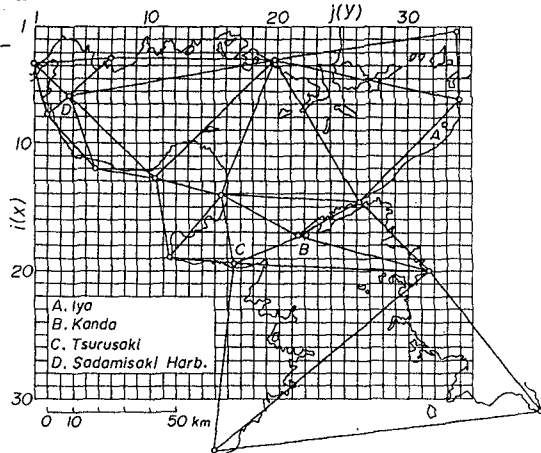


Fig. 9 Grid system used in the western part of the Seto Inland Sea.

correspondence of the computation with the observation is excellent through all periods of the storm, and reasonable agreement between them is also achieved at Iyo with longer fetch, though the observed results are limited in a short period under high wave conditions. The reason why the observed wave periods are slightly greater than the computed ones may be due to the fact that the observation was made with a pressure-type wave gauge.

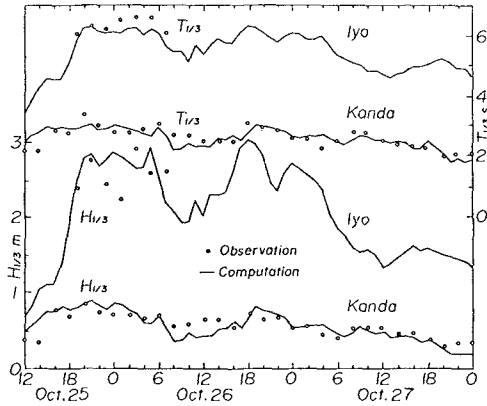


Fig. 10 Comparison between the computed and observed significant waves at Iyo and Kanda.

(5) Wave Hindcast in the Japan Sea

Fig. 10 is the grid system with spacing of 40 km used in wave hindcast on the Japan Sea. The winter storm of interest was generated by a low system whose time history was that two lows, one proceeding northeasterly along the Japan Sea and the other similarly along the Pacific Ocean side of the Japanese coast, came together over the eastern sea area of north Japan and the central pressure lowered to 970 mb at the severest period. Wind distribution over the area is given by the method (Yamaguchi et al., 1984) which estimates gradient winds by approximating curvature of the isobar line and pressure gradient with a spline function and then converts them to winds over the sea, multiplying a constant coefficient(=0.67) by gradient wind velocity and rotating gradient wind direction by 17° counter-clockwise.

The computed and observed time variations of significant waves at

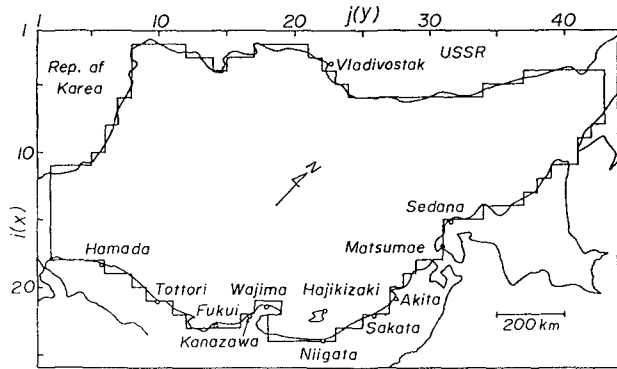


Fig. 11 Grid system used in the Japan Sea.

Wajima with a water depth of 50 m and Tottori with a water depth of 30 m are compared in Fig. 12. The model takes into account the effect of water depth on waves in an expedient way by multiplying the frequency spectrum computed at the hindcast point by a correction factor of $\Phi(kh)=\tanh^2 kh$, where k is the wave number and h the water depth. DOLPHIN-I with a correction for water depth effect predicts the variation of waves with the change of winds in a general sense better than the original DOLPHIN-I, but the degree of agreement between the computation and the observation is not as accurate as in the above-mentioned cases in which wind distribution is estimated with interpolation of measured wind data, because of less accuracy of hindcast winds. In particular, the computed time variation of waves at Wajima is about 4 hours behind the observed one, reflecting the time lag between the computed winds and the measured winds.

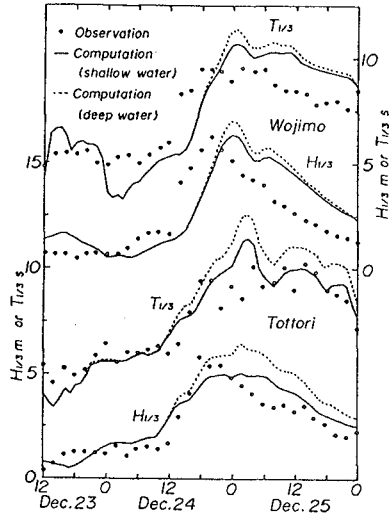


Fig. 12 Comparison between the computed and observed significant waves at Wajima and Tottori.

(6) Wave Hindcast in the Northwest Pacific Ocean

Waves caused by a typhoon with rapidly-varying wind fields is hindcast in the Pacific Ocean. Fig. 13 is the grid system with a spacing of 80 km placed on the Pacific Ocean, in which the tracks of two typhoons to be hindcast for wave conditions - Typhoon 8115 and Typhoon 8210 - are also drawn. The estimation of wind distribution in a typhoon relies on the use of a parametric typhoon model. The model in which the exponential function is assumed for the pressure distribution, computes the wind fields in a typhoon

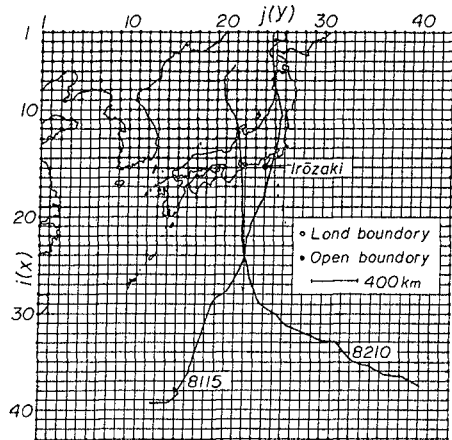


Fig. 13 Grid system used in the Pacific Ocean.

by using parameters such as central pressure, position of the typhoon center, radius to maximum winds and wind inflow angle to the typhoon center. These data are given every 6 hours and through a linear interpolation, wind field is estimated at intervals of 1 hour.

Fig. 14 is the time variation of significant waves at Irouzaki situated on the Pacific Ocean side of the Japanese coast, as is indicated in Fig. 13. The computation is in close agreement with the observation showing propagation of swell with a distant typhoon and rapid growth and decay of wind waves with approach and passage of a typhoon. Accordingly, the model predicts general characteristics of typhoon-generated waves in the northern hemisphere such that waves during Typhoon 8210 when Irouzaki was situated on the right hand side of the typhoon track give more rapid growth and decay associated with approach and passage of a typhoon than those during Typhoon 8115 when Irouzaki was situated on the left hand side of the typhoon track. When the effect of water depth on wave characteristics at Irouzaki where water depth is 50 m deep is introduced in the same way as in the Japan Sea case, the computed results might be slightly smaller than the observed ones.

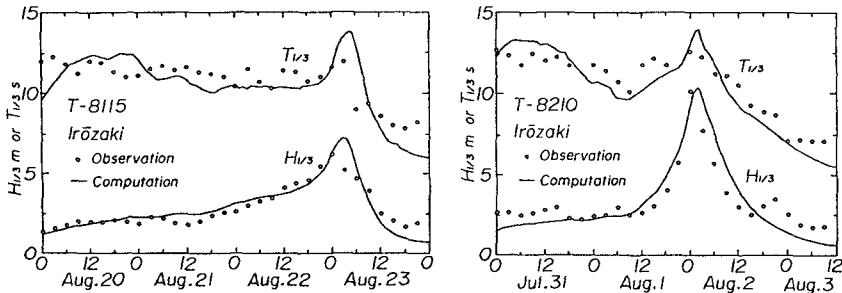


Fig. 14 Comparison between the computed and observed significant waves at Irouzaki.

4. CONCLUSIONS

Practical applicability of the wave prediction model developed by the authors, DOLPHIN-1, was confirmed by reasonable agreement between the hindcast results and the wave data, including directional spectrum, which were acquired in five sea areas with different horizontal scales around Japan.

5. ACKNOWLEDGEMENTS

The authors thank the Bureaus of Harbor Construction, Ministry of Transportation and the Prefectural Offices for kindly offering the valuable wind and wave data.

REFERENCES

- Graber, H.C. and Madsen, O.S. (1988): A finite-depth wind-wave model, Part 1-Model description, *J. Phys. Oceanogr.*, Vol.18, pp. 1465 - 1483.
- Günther, H., Komen, G.J. and Rosenthal, W. (1984): A semi-operational comparison of two parametrical wave prediction models, *Deutsch. Hydrogr. Zeit.*, No. 37, Heft 3, pp. 89-106.
- Hasselmann, K. et al. (1973): Measurements of wind-wave growth and swell decay during the Joint North Sea Wave Project(JONSWAP), *Deutsch. Hydrogr. Zeit.*, A8, Heft 12, pp. 1 - 95.
- Mitsuyasu, H. et al. (1980): Observation of the power spectrum using a cloverleaf buoy, *J. Phys. Oceanogr.*, Vol. 10, pp. 286 - 296.
- Mitsuyasu, H. and Kusaba, T. (1984): Drag coefficient over water surface under the action of strong wind, *J. Natural Disas. Sci.*, Vol. 6, No. 2, pp. 43 - 50.
- Ross, D.B. (1976): A simplified model for forecasting hurricane generated waves (abstract), *Bull. American Meteorol. Soc.*, No. 113.
- SWAMP Group (1985): *Ocean Wave Modeling*, Plenum Press, 256pp.
- Yamaguchi, M. et al. (1981): Spatial distribution of winds over Osaka Bay, *Proc. 28th Conf. on Coastal Eng. in Japan*, pp.168 - 172 (in Japanese).
- Yamaguchi, M. et al. (1984): A method for estimating surface winds from weather map analysis based on spline function approximation, *Proc. 31st Conf. on Coastal Eng. in Japan*, pp. 128 - 132 (in Japanese).
- Yamaguchi, M., Holthuijsen, L.H., Hatada Y. and Hino, M. (1988): A new hybrid parametric wave prediction model taking the wave directionality into account, *Proc. JSCE*, Vol. 399/II-10, pp. 193-202 (in Japanese).